Small molecule-facilitated anion transporters for a novel cystic fibrosis substitutive therapy

SUPPLEMENTARY DATA

Michele Fiore[1], Claudia Cossu[1], Valeria Capurro[2], Cristiana Picco[1], Alessandra Ludovico[1], Marcin Mielczarek[3], Israel Carreira-Barral[3], Emanuela Caci[2], Debora Baroni[1], Roberto Quesada[3], Oscar Moran[1*]

[1]Istituto di Biofisica, CNR, Genova, Italy;
[2]U.O.C. Genetica Medica, Istituto Giannina Gaslini, Genova, Italy
[3]Departamento de Química, Facultad de Ciencias, Universidad de Burgos, Burgos, Spain

Table of Contents

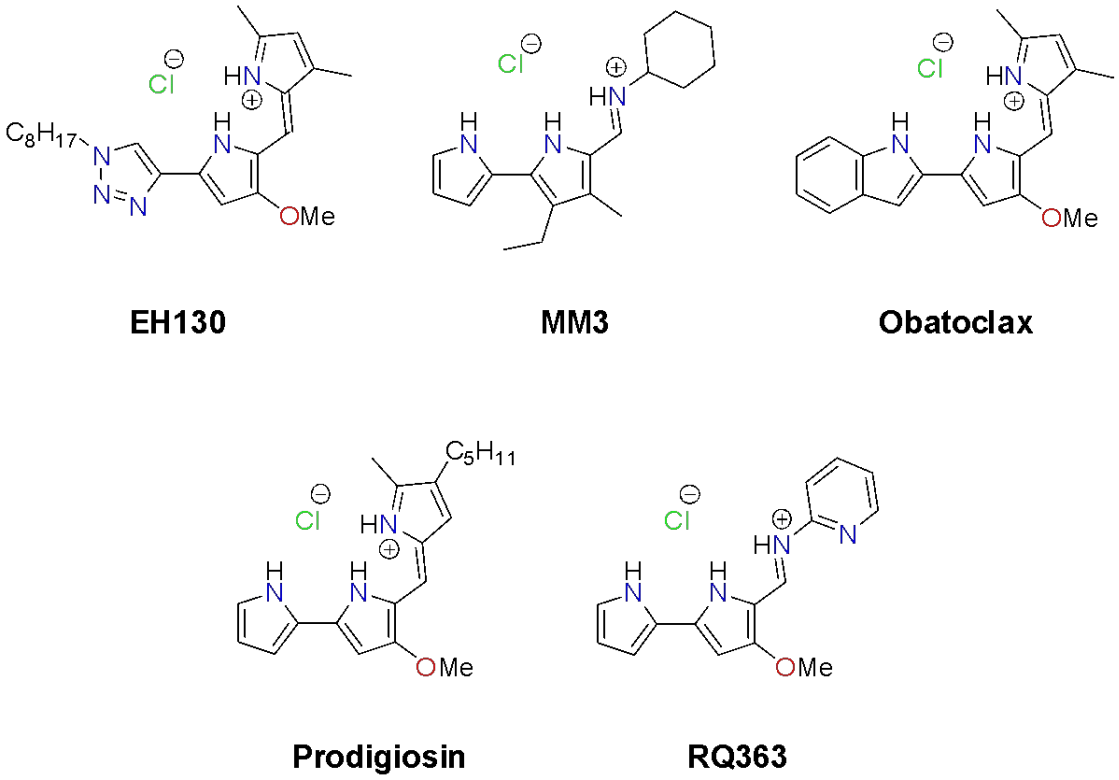

Figure S1. Structures of the studied compounds.

Synthesis and characterisation of compound MM3

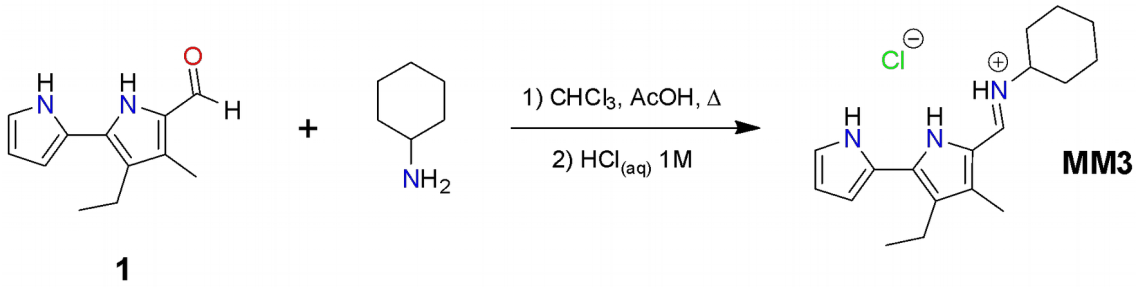

1

Aldehyde **1** was prepared according to the literature (Kancharla and Reynolds 2013). To a solution of such aldehyde (250.9 mg, 1.24 mmol) in chloroform (10 ml) glacial acetic acid (50 µl) and cyclohexylamine (275 µl, 2.40 mmol, 1.94 equiv.) were added, and the resulting reaction mixture was stirred at 60 °C for 6 h. Upon cooling to room temperature the chloroform was evaporated under reduced pressure and the residue was re-dissolved in dichloromethane (30 ml). The solution of the crude compound **MM3** was washed with 1 M aqueous HCl solution (3 × 20 ml), dried over anhydrous Na_2SO_4, filtered and evaporated to dryness under reduced pressure. The residue was recrystallised from a mixture of dichloromethane and *n*-hexane to give compound **MM3** as dark green needles (264.2 mg, 67%). ^{1}H NMR (300 MHz, $CDCl_3$): δ (ppm) = 13.59 (s, 1H), 10.83 (s, 1H), 10.30 (d, 1H, *J* = 15 Hz), 7.38 (d, 1H, *J* = 15 Hz), 7.12-7.08 (m, 1H), 6.81-6.76 (m, 1H), 6.34-6.28 (m, 1H), 3.52-3.36 (m, 1H), 2.66 (q, 2H, *J* = 7.5 Hz), 2.19 (s, 3H), 2.13-2.03 (m, 2H), 1.97-1.84 (m, 2H), 1.76-1.60 (m, 2H), 1.43-1.22 (m, 4H), 1.15 (t, 3H, *J* = 7.5 Hz). ^{13}C NMR (75 MHz, $CDCl_3$): δ (ppm) = 141.6 (CH), 139.1 (ArC), 139.0 (ArC), 126.4 (ArC), 122.6 (ArCH), 122.3 (ArC), 119.6 (ArC), 112.1 (ArCH), 110.4 (ArCH), 60.0 (CH), 33.0 (CH_2), 24.4 (CH_2), 24.2 (CH_2), 17.7 (CH_2), 13.4 (CH_3), 9.0 (CH_3). HR-MS (ESI^+): found *m/z* (Da) = 284.2121 $[C_{18}H_{26}N_3]^+$; calculated *m/z* (Da) = 284.2121.

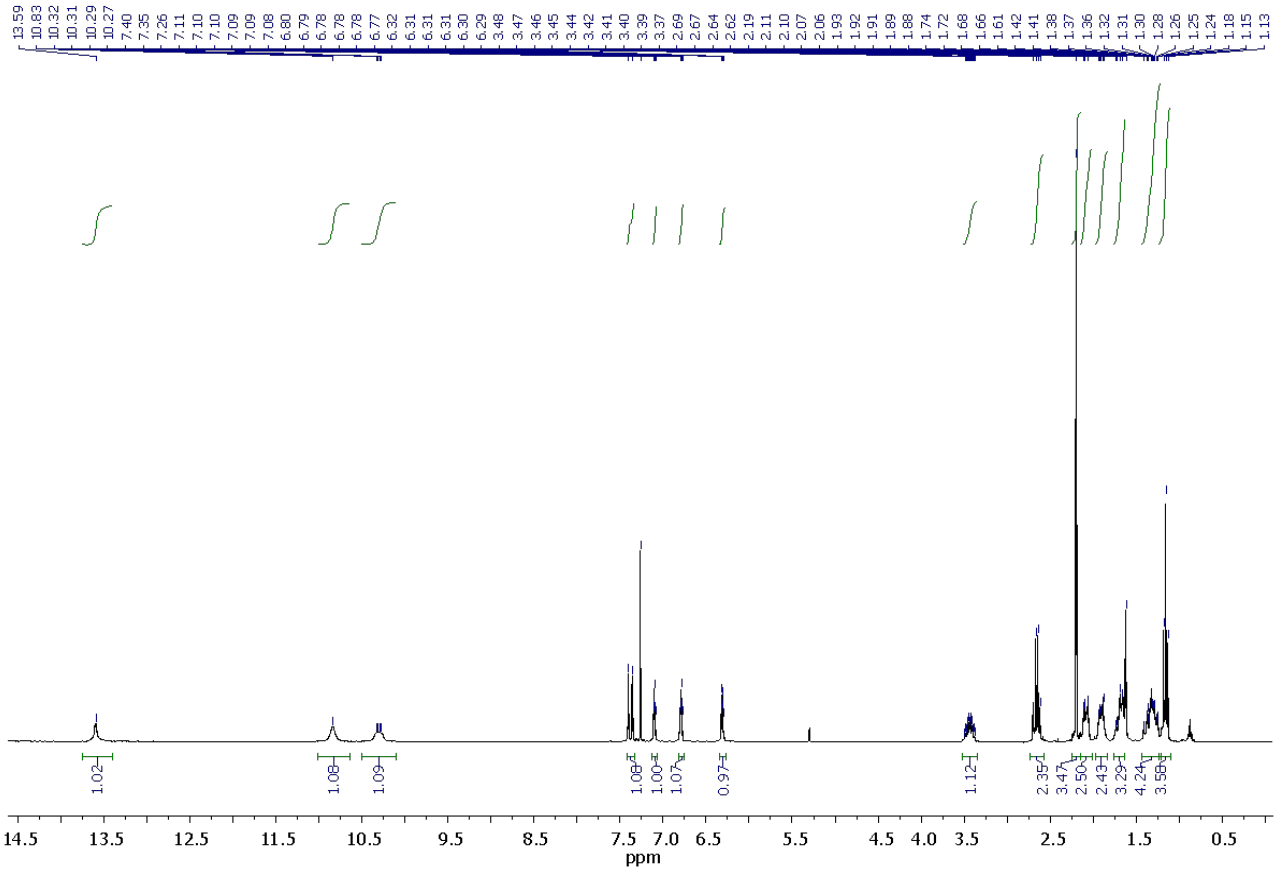

Figure S2. ^{1}H NMR spectrum (300 MHz, $CDCl_3$) for compound **MM3**.

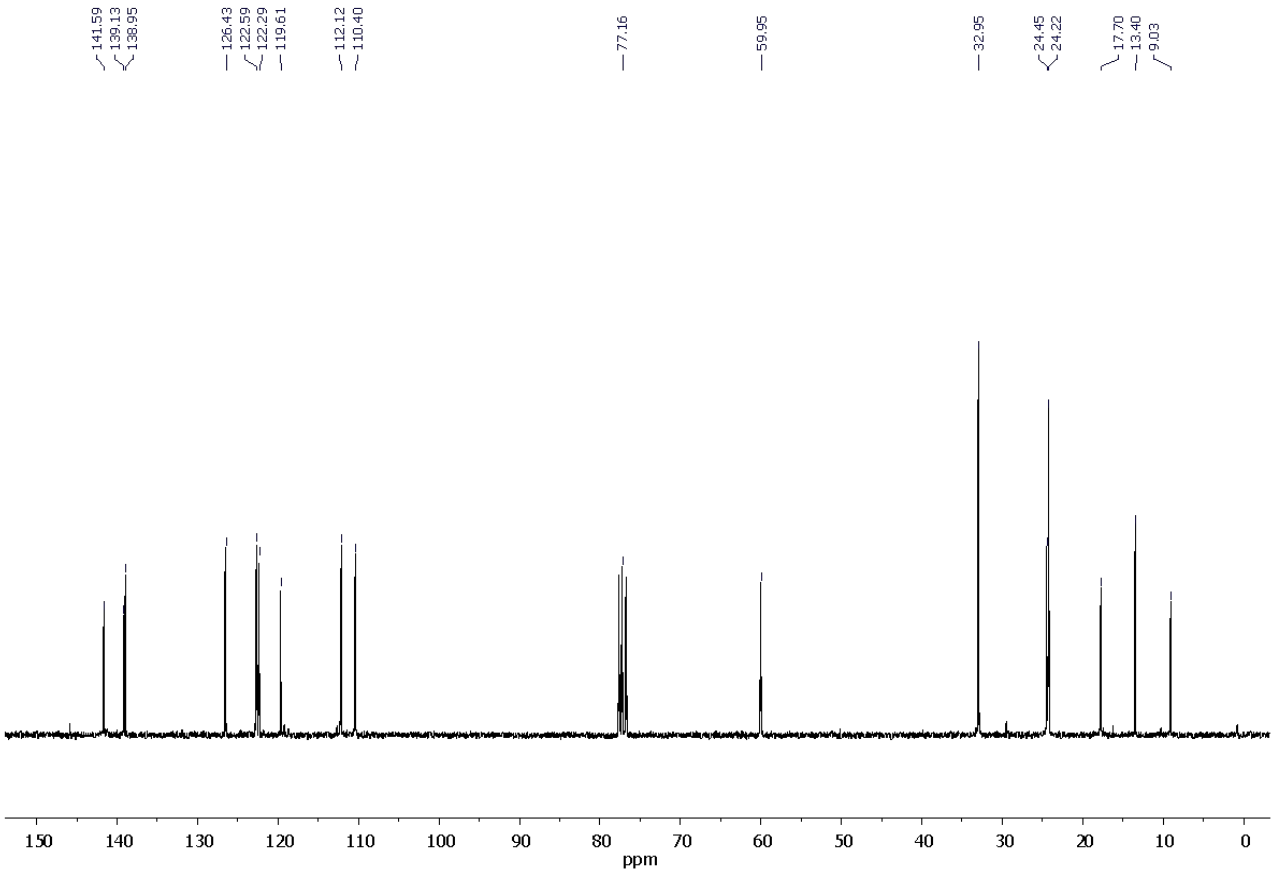

Figure S3. ^{13}C NMR spectrum (75 MHz, $CDCl_3$) for compound **MM3**.

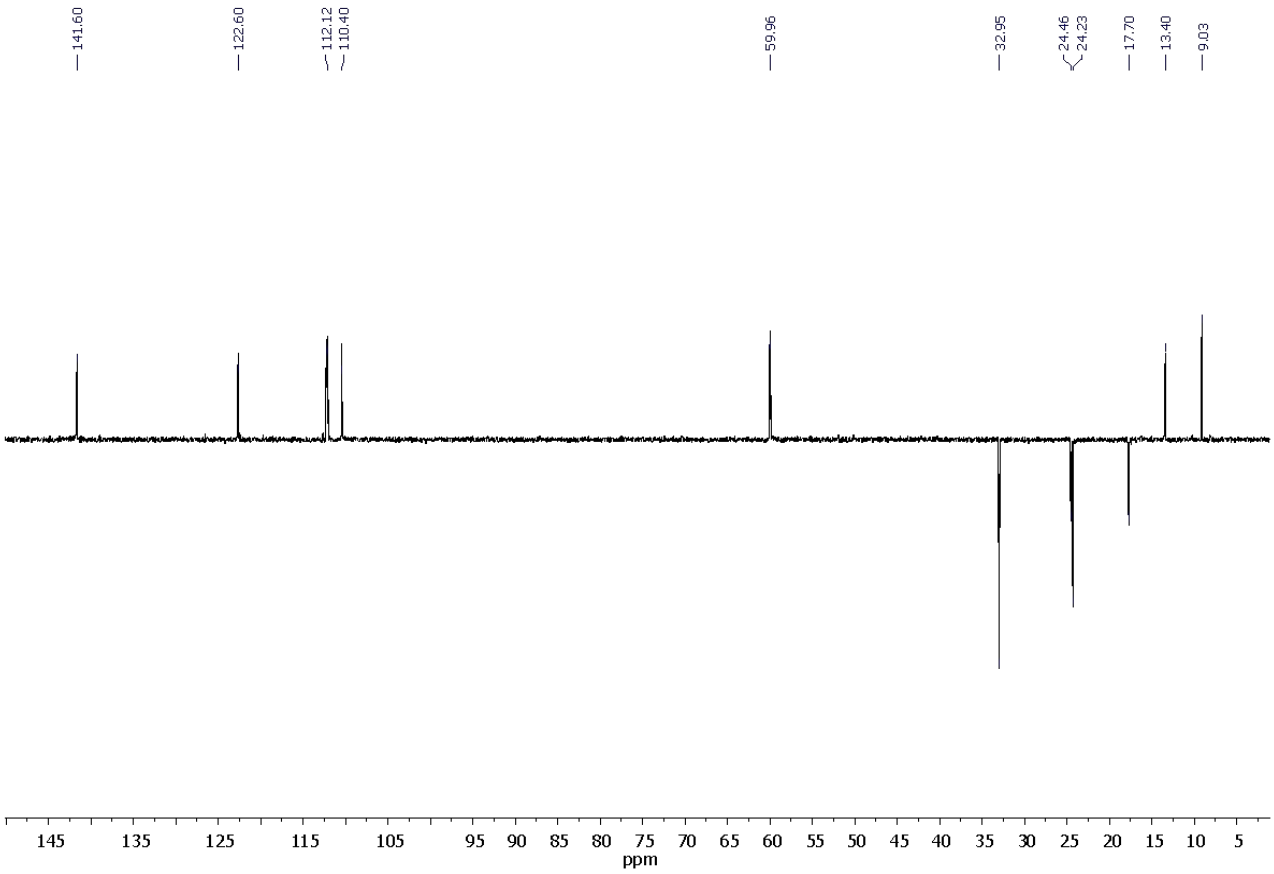

Figure S4. ^{13}C NMR dept135 spectrum (75 MHz, $CDCl_3$) for compound **MM3**.

Figure S5. HR-MS (ESI^+) spectra for compound **MM3.**

X-RAY DIFFRACTION STUDIES

Solid state structure of compound MM3

Single crystals were obtained by slow evaporation of a solution of the isolated compound in a 1:1 dichloromethane-methanol mixture.

Three dimensional X-ray data were collected on a BRUKER SMART APEX CCD diffractometer. Complex scattering factors were taken from the program SHELX-97 (Hübschle et al. 2011) running under the WinGX program system (Farrugia 1999) as implemented on a Pentium computer. The structure was solved with SIR97 (Altomare et al. 1999) and refined by full-matrix least-squares on F^2. All hydrogen atoms, except those corresponding to the NH fragments of the imine function and the pyrrole and indole rings, which were refined freely, were included in calculated positions and refined in riding mode. Refinement converged with anisotropic displacement parameters for all non-hydrogen atoms. Crystal data and details on data collection and refinement are summarised in Table 1.

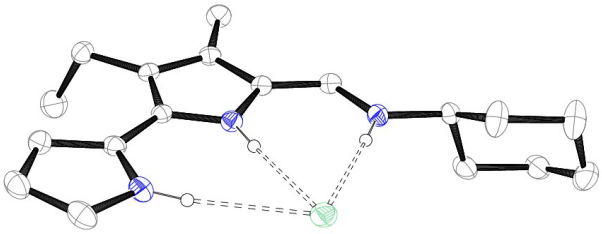

Figure S6. X-ray structure of compound **MM3**. Hydrogen atoms, except those involved in hydrogen-bonding interactions, are omitted for the sake of simplicity. The ORTEP plot is at the 30% probability level.

Table 1. Crystal data and refinement details for **MM3**.

formula	$C_{18}H_{26}ClN_3$	Z	18
MW	319.87	λ, Å (MoK$_\alpha$)	0.71073
crystal system	Trigonal	D_{calc}/g cm^{-3}	1.128
space group	R -3	μ/mm^{-1}	0.204
T/K	100(2)	θ range/deg	1.38 – 28.26
a/Å	29.4497(19)	R_{int}	0.1326
b/Å	29.4497(19)	reflections measured	32843
c/Å	11.2815(15)	unique reflections	4455
α/deg	90	reflections observed	2773
ß/deg	90	GOF on F^2	0.988
γ/deg	120	$R1^a$	0.0576
V/Å^3	8473.4(16)	$wR2^b$	0.1439
F(000)	3096	Largest ≠ peak & hole/eÅ^{-3}	0.506 and -0.399

$$^{a}\ R1=\frac{\sum|F_0-F_C|}{\sum|F_0|}\ ;\ ^{b}\ wR2=\left[\frac{\sum\left[w\left(F_0^2-F_C^2\right)^2\right]}{\sum\left[w\,F_0^4\right]}\right]^{1/2}$$

Anion exchange experiments (Cl^-/NO_3^-) in unilamelar vesicles

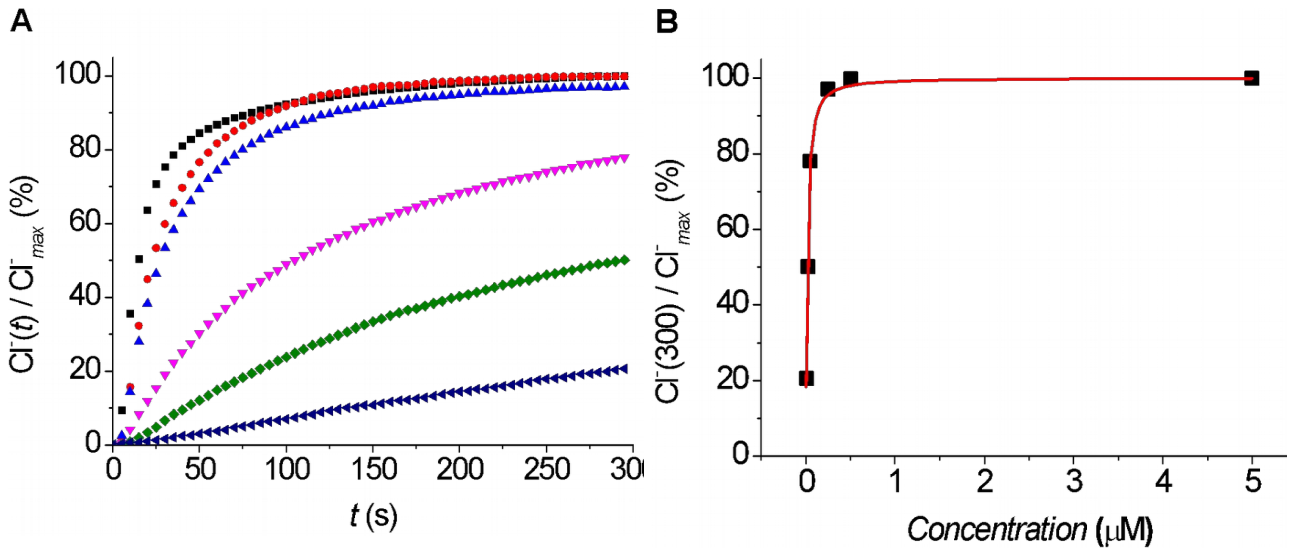

Figure S7. A: Chloride efflux promoted by EH130 at different concentrations (5 μM, black; 0.5 μM, red; 0.25 μM, light blue; 0.05 μM, magenta; 0.02 μM, green; 0.005 μM, dark blue) in LUV. Vesicles loaded with 489 mM NaCl were buffered at pH 7.2 with 5 mM phosphate and dispersed in 489 mM $NaNO_3$ buffered at pH 7.2. Each trace represents the average of three independent mesurements. **B:** The normalised chloride efflux at 300 s plotted against the anionophore concentration. The dose-response curve iwas constructed from 144 independent measurements. Data have been plotted with Hill equation (continuous line), yielding an ED_{50} of 0.018 μM.

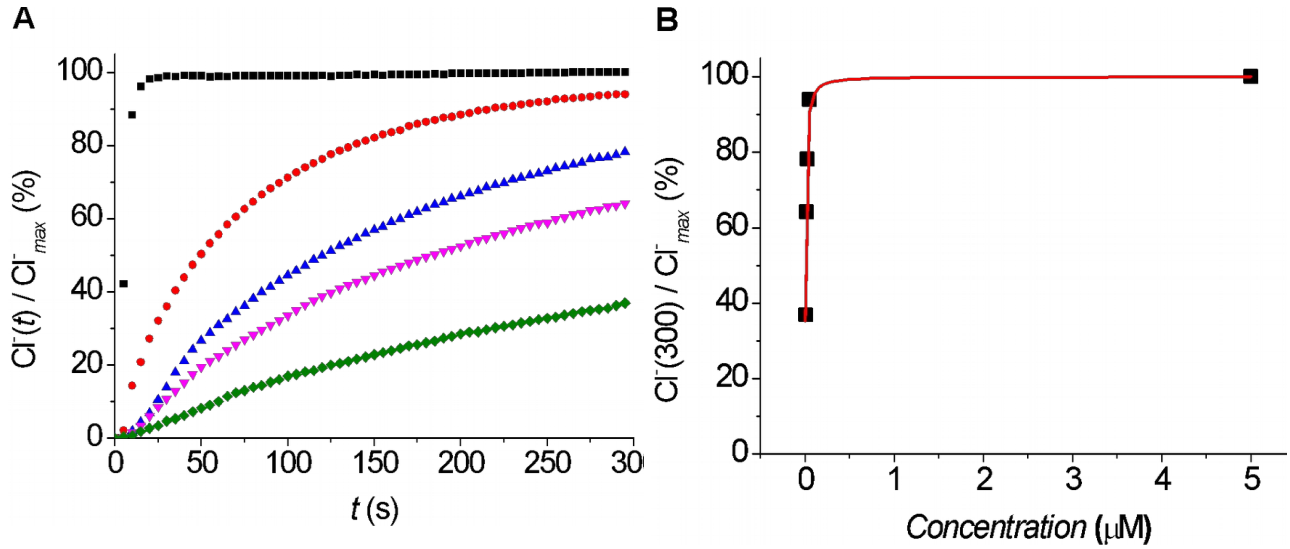

Figure S8. A: Chloride efflux promoted by MM3 at different concentrations (5 μM, black; 0.05 μM, red; 0.025 μM, blue; 0.015 μM, magenta; 0.005 μM, green) in LUV. Vesicles loaded with 489 mM NaCl were buffered at pH 7.2 with 5 mM phosphate and dispersed in 489 mM $NaNO_3$ buffered at pH 7.2. Each trace represents the average of three independent mesurements. **B:** The normalised chloride efflux at 300 s plotted against the anionophore concentration. The dose-response curve iwas constructed from 15 independent measurements. Data have been plotted with Hill equation (continuous line), yielding an ED_{50} of 0.0083 μM.

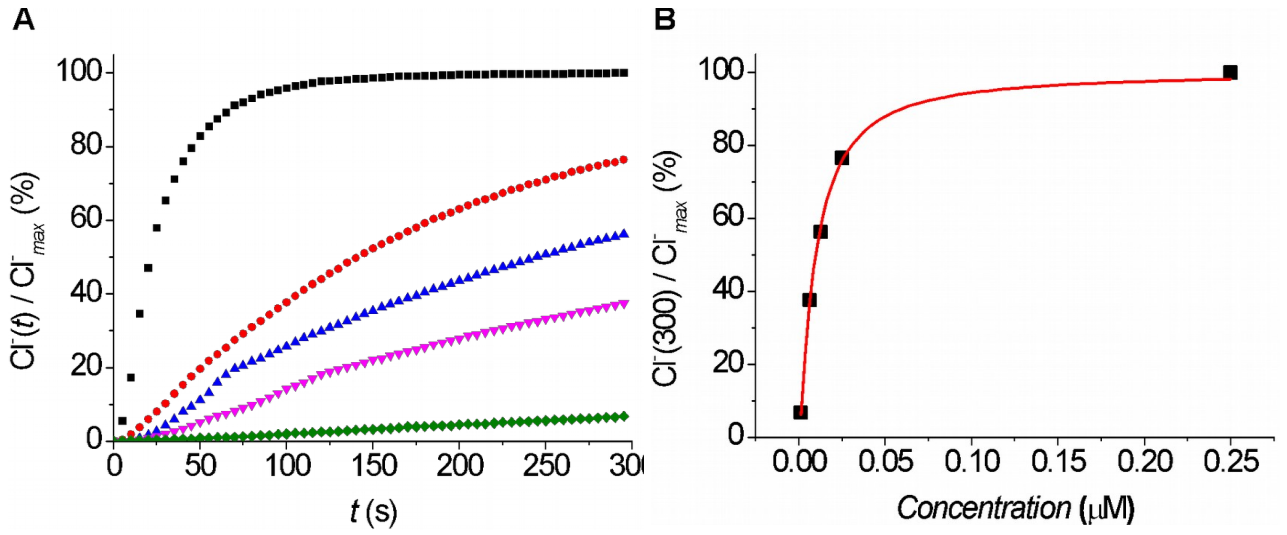

Figure S9. A: Chloride efflux promoted by Obatoclax at different concentrations (0.25 μM, black; 0.025 μM, red; 0.0125 μM, blue; 0.00625 μM, magenta; 0.001 μM, green) in LUV. Vesicles loaded with 489 mM NaCl were buffered at pH 7.2 with 5 mM phosphate and dispersed in 489 mM $NaNO_3$ buffered at pH 7.2. Each trace represents the average of three independent mesurements. **B:** The normalised chloride efflux at 300 s plotted against the anionophore concentration. The dose-response curve iwas constructed from 90 independent measurements. Data have been plotted with Hill equation (continuous line), yielding an ED_{50} of 0.0097 μM.

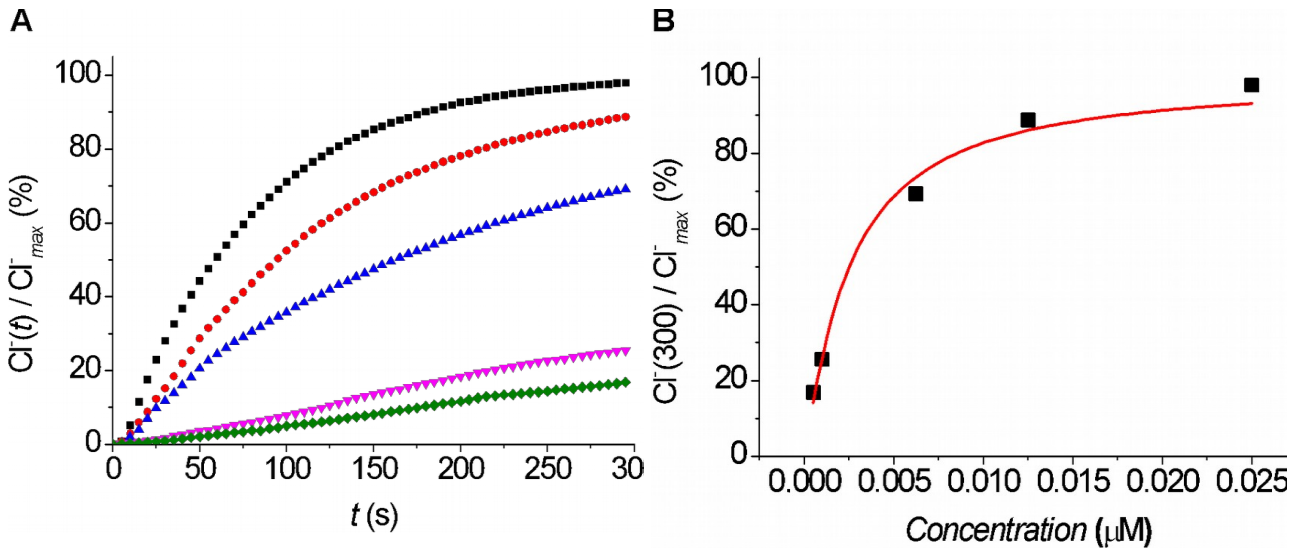

Figure S10. A: Chloride efflux promoted by Prodigiosin at different concentrations (0.025 μM, black; 0.0125 μM, red; 0.00625 μM, blue; 0.001 μM, magenta; 0.0005 μM, green) in LUV. Vesicles loaded with 489 mM NaCl were buffered at pH 7.2 with 5 mM phosphate and dispersed in 489 mM $NaNO_3$ buffered at pH 7.2. Each trace represents the average of three independent mesurements. **B:** The normalised chloride efflux at 300 s plotted against the anionophore concentration. The dose-response curve iwas constructed from 15 independent measurements. Data have been plotted with Hill equation (continuous line), yielding an ED_{50} of 0.0025 μM.

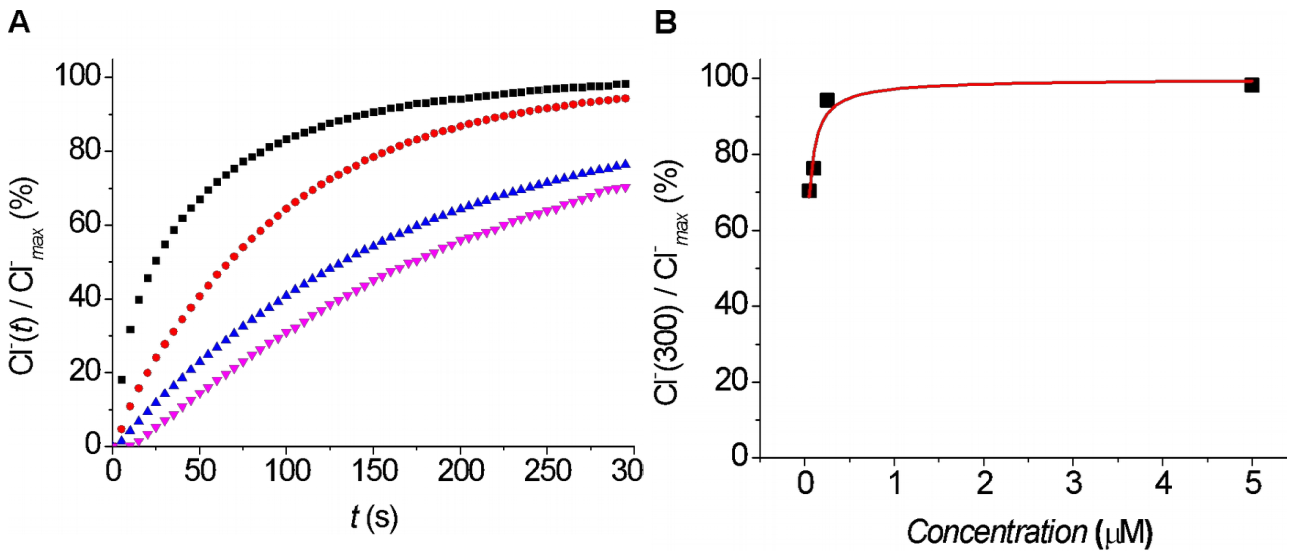

Figure S11. A: Chloride efflux promoted by RQ363 at different concentrations (5 μM, black; 0.25 μM, red; 0.1 μM, blue; 0.05 μM, magenta) in LUV. Vesicles loaded with 489 mM NaCl were buffered at pH 7.2 with 5 mM phosphate and dispersed in 489 mM $NaNO_3$ buffered at pH 7.2. EEach trace represents the average of three independent mesurements. **B:** The normalised chloride efflux at 300 s plotted against the anionophore concentration. The dose-response curve iwas constructed from 36 independent measurements. Data have been plotted with Hill equation (continuous line), yielding an ED_{50} of 0.021 μM.

Experiments in cells

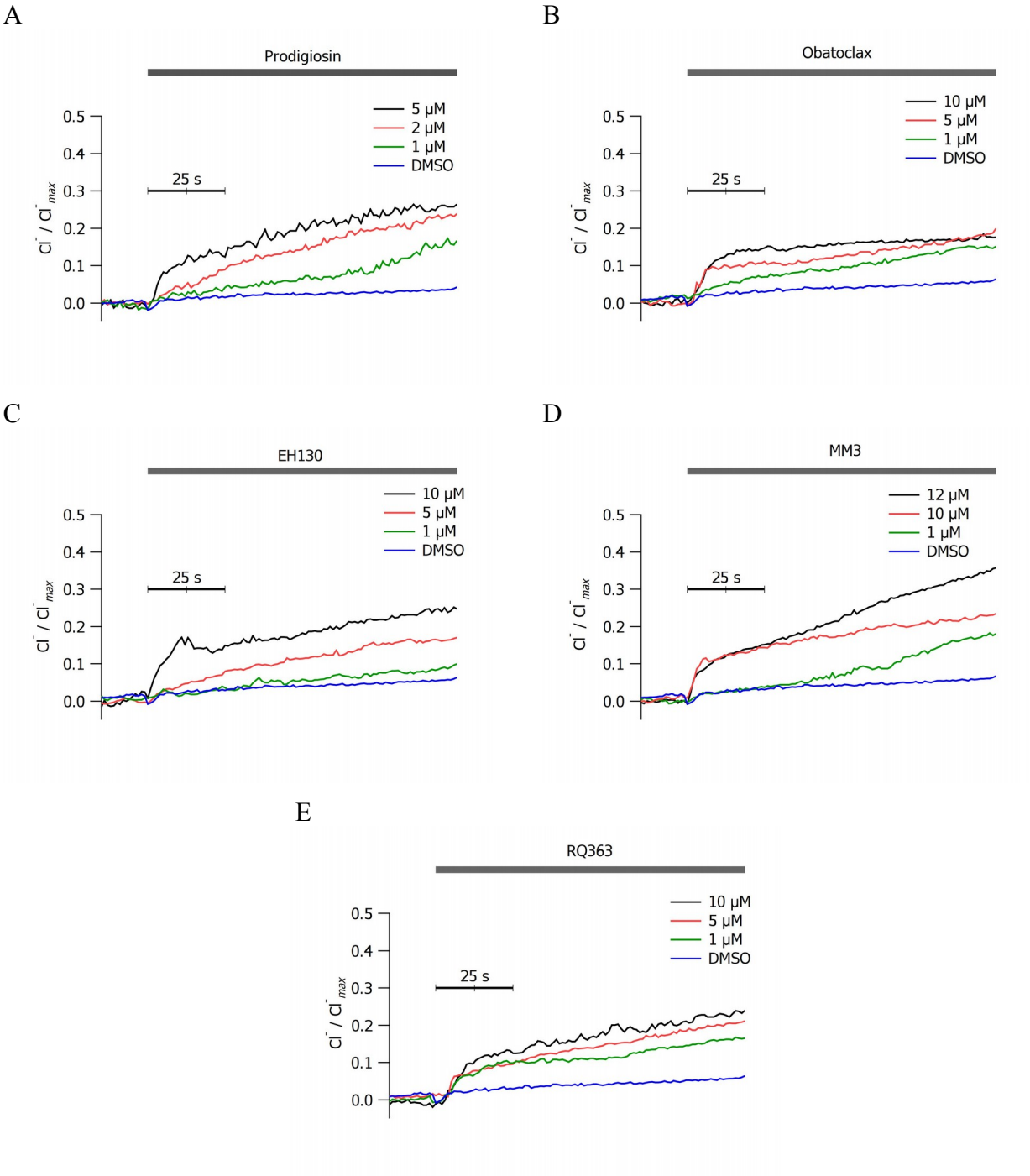

Figure S12. Chloride efflux measured in CHO cells upon addition of different concentrations of prodigiosines (**A-C**) and tambjamines (**D-E**), as indicated in the figure. The application the anionophores are indicated by the upper bar.

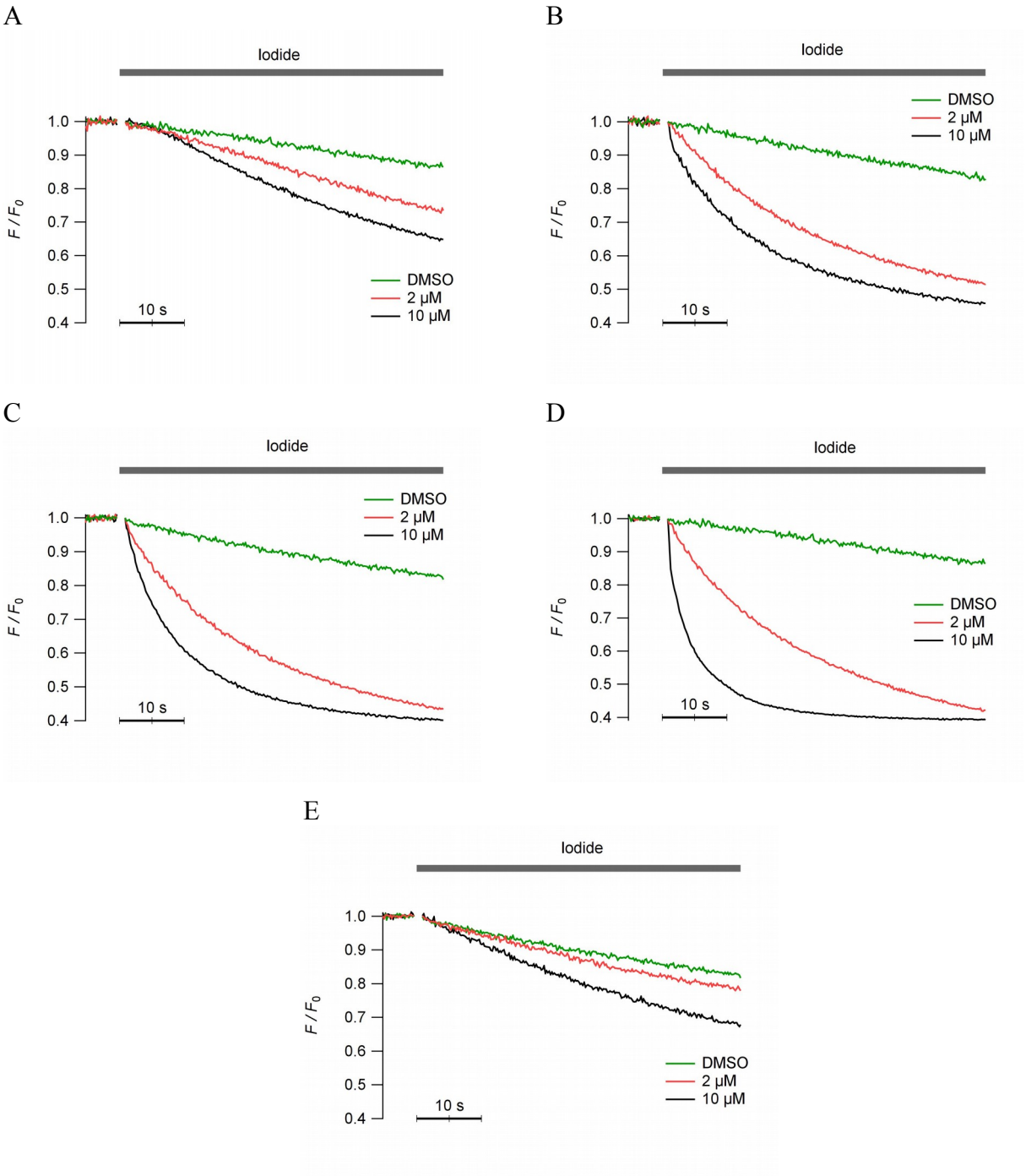

Figure S13. Iodide influx assay in FRT cells. Figure indicate the time course of the fluorescence decay in FRT cells incubated at different concentration of EH130 (**A**), Prodigiosin (**B**), obatoclax (**C**), MM3 (**D**), RQ363 (**E**). The Iodide injection are indicated by the upper bar.

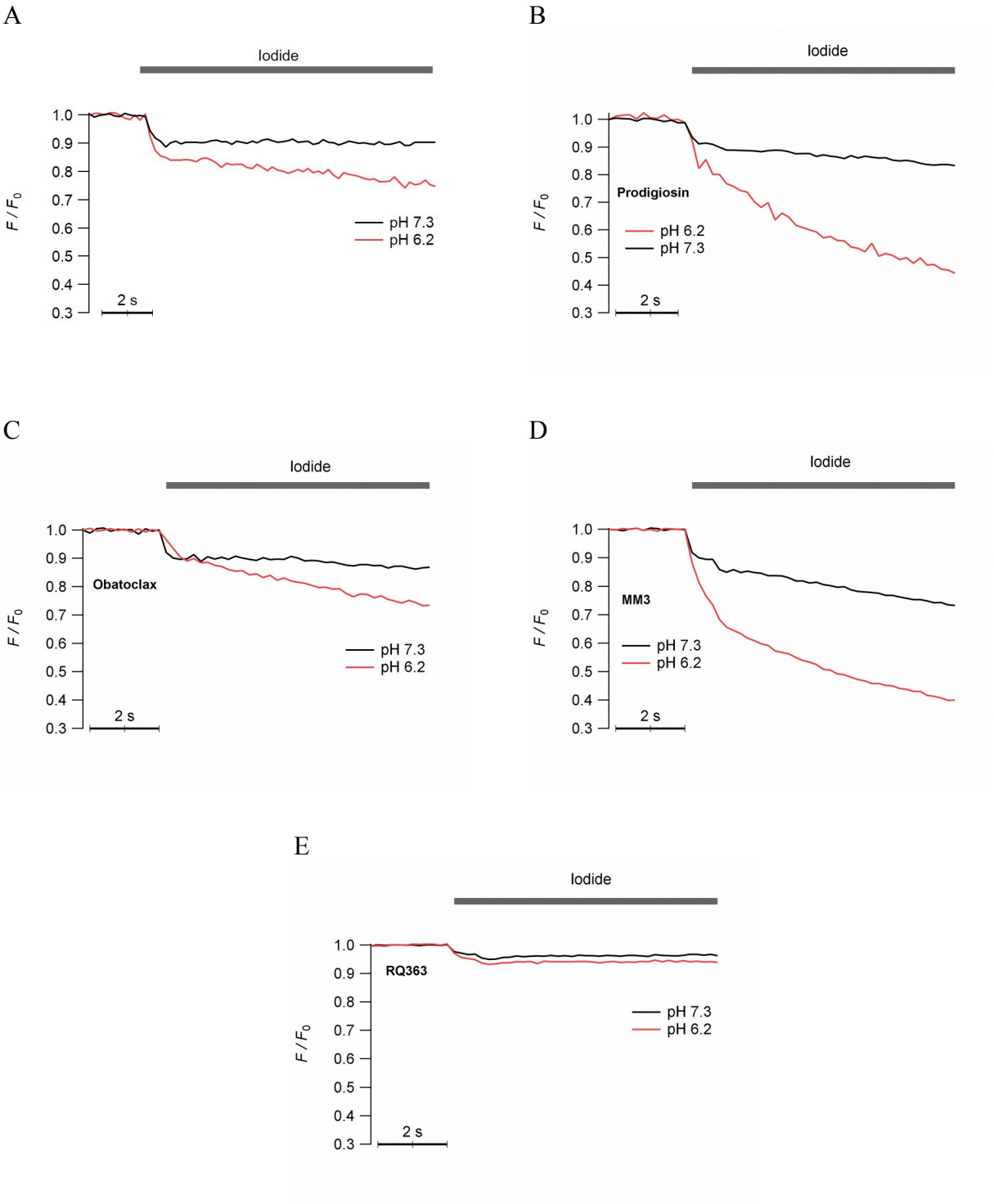

Figure S14. Effects of pH on anionophores activity. Figure indicate the time course of the fluorescence decay in FRT cells incubated with 2 μM. The Iodide injection are indicated by the upper bar. The traces indicate iodide transport using 2 different pH values of extracellular solution.

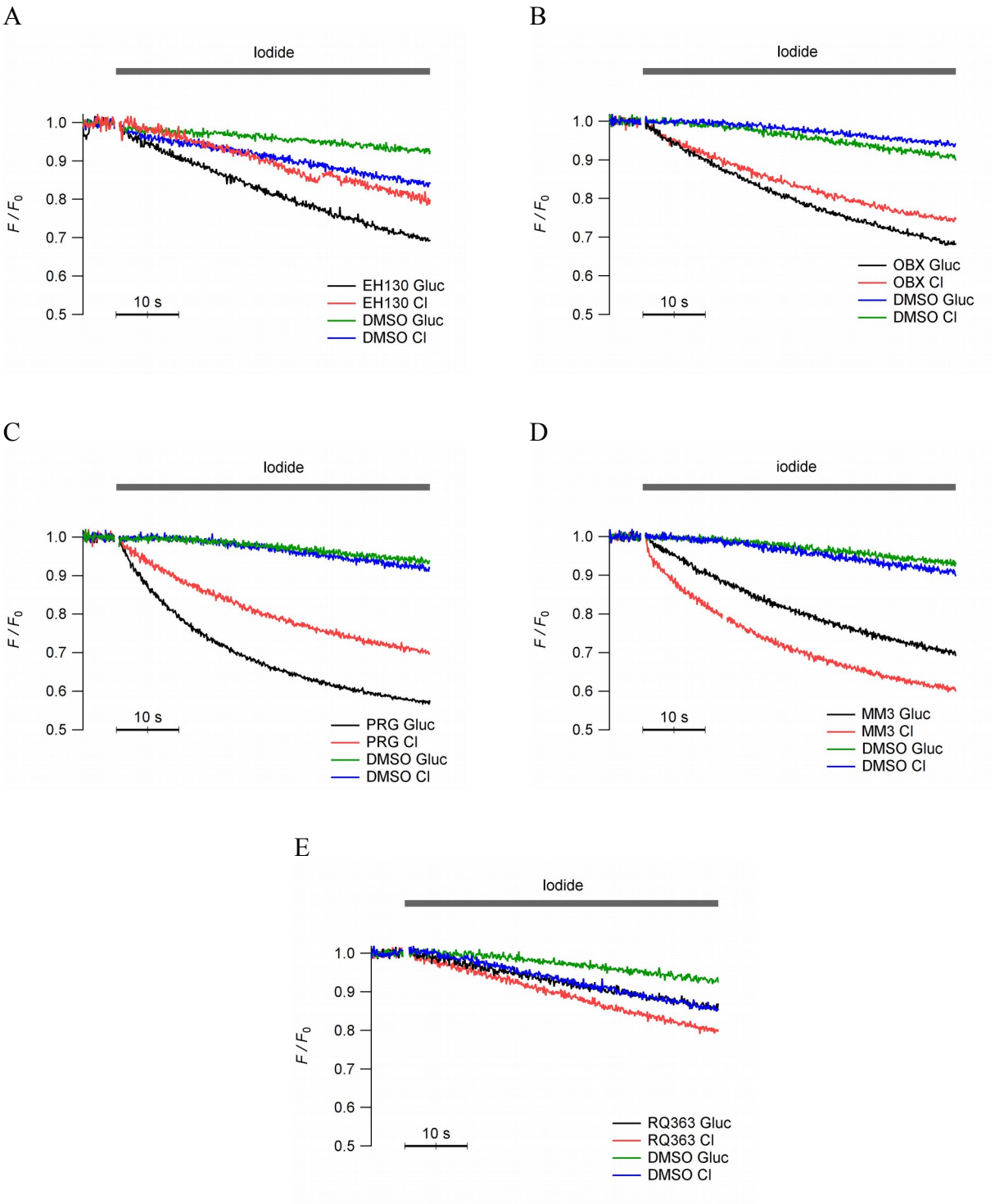

Figure S15. Effects of anion competition in iodide transport. Figure indicate the time course of the fluorescence decay in FRT cells incubated with 2 μM of anionophores. Iodide transport was measured with different concentrations of chloride and gluconate in the extracellular solution.

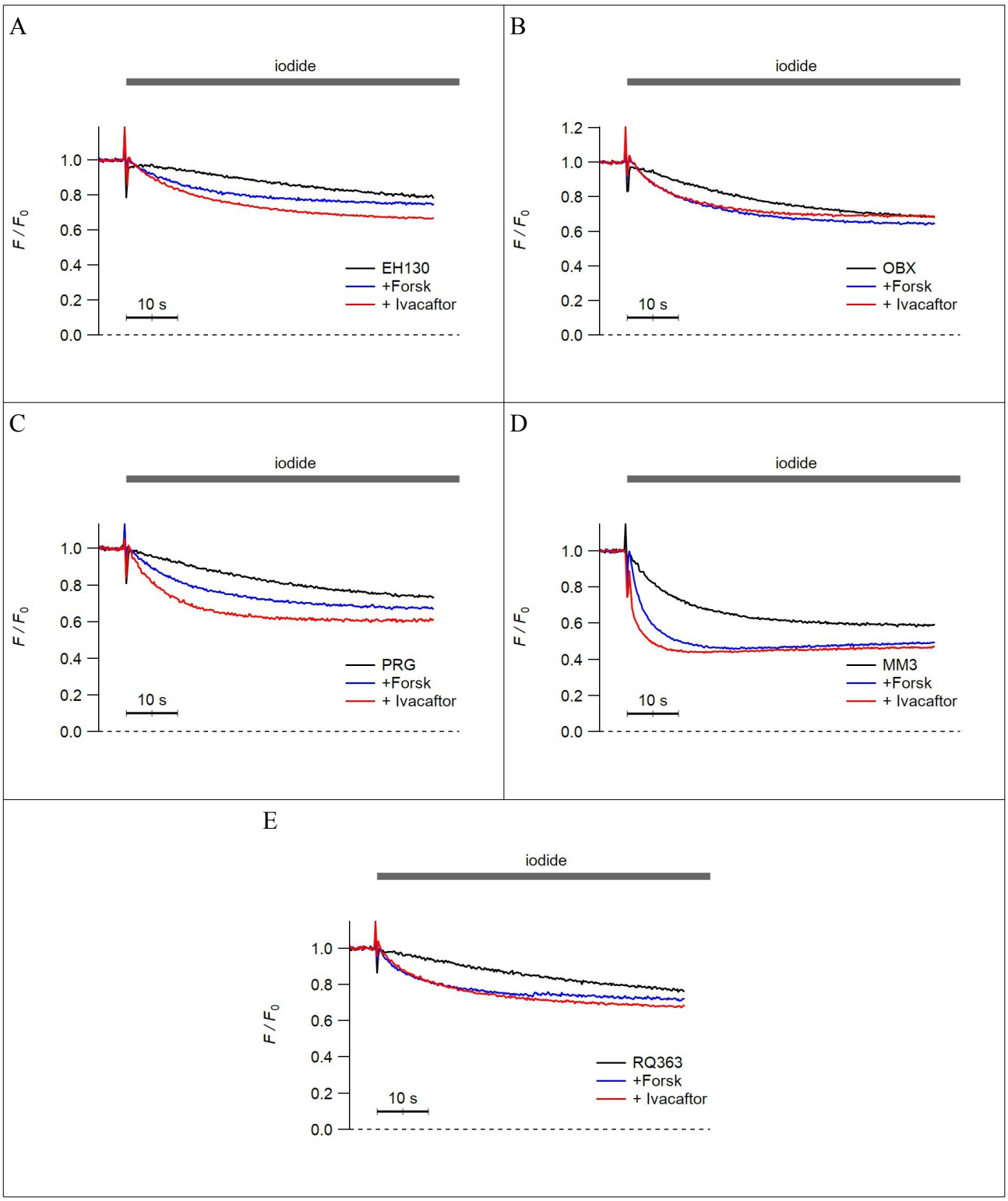

Figure S16. Anionophore-driven iodide transport in cells transfected with WT CFTR. Figure indicate the time course of the fluorescence decay in CFTR transfected FRT cells incubated with 2 μM of anionophores. Iodide transport was measured after incubation with anionipore (black trace), anionophore plus forskolin that activates the CFTR (blue trace) and in cells treated with anionophore, forskolin and the CFTR potentiator Ivacaftor (red line).

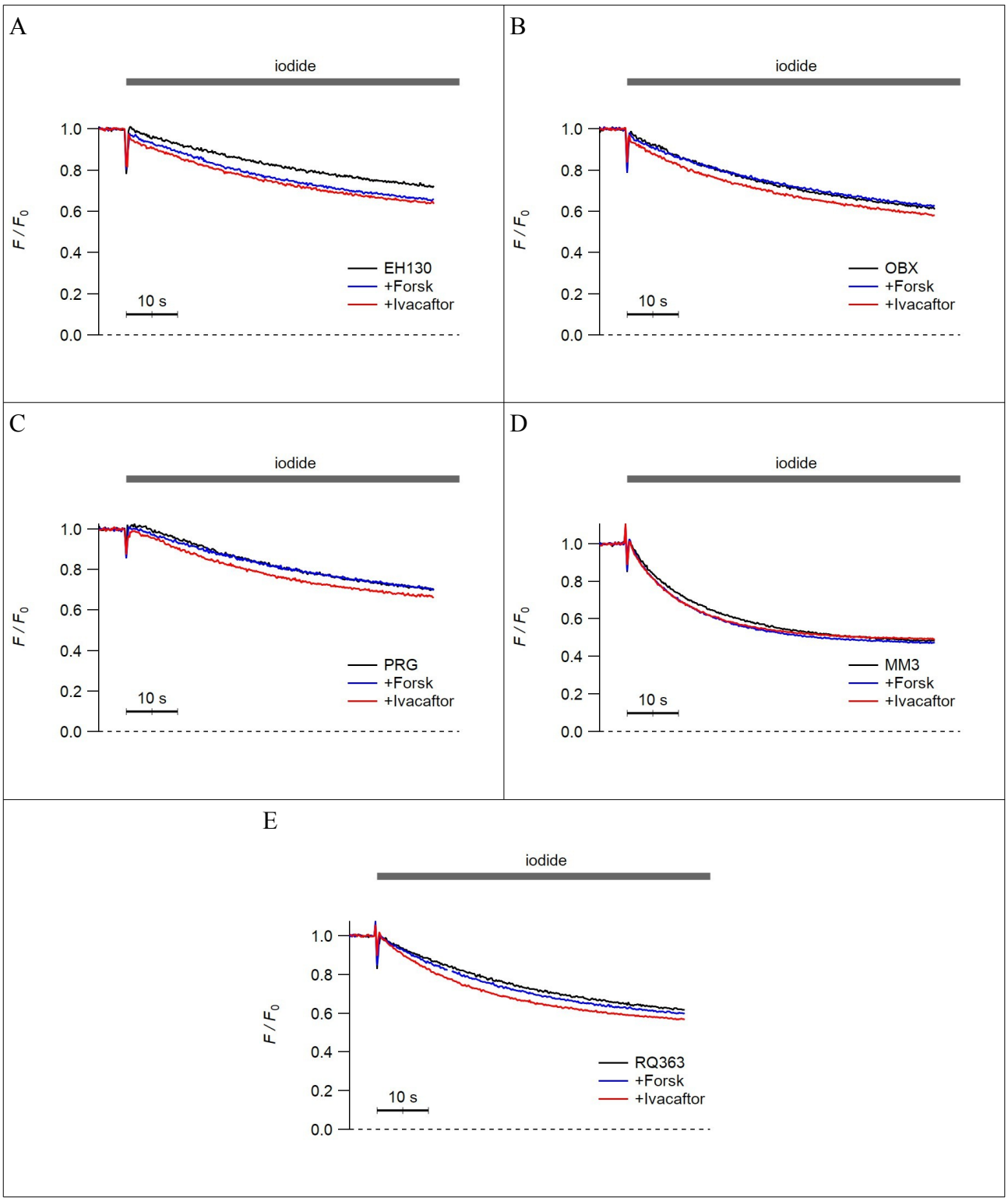

Figure S17. Anionophore-driven iodide transport in cells transfected with G551D CFTR. Figure indicate the time course of the fluorescence decay in mutant-CFTR transfected FRT cells incubated with 2 μM of anionophores. Iodide transport was measured after incubation with anionipore (black trace), anionophore plus forskolin that activates the mutant-CFTR (blue trace) and in cells treated with anionophore, forskolin and the CFTR potentiator Ivacaftor (red line).

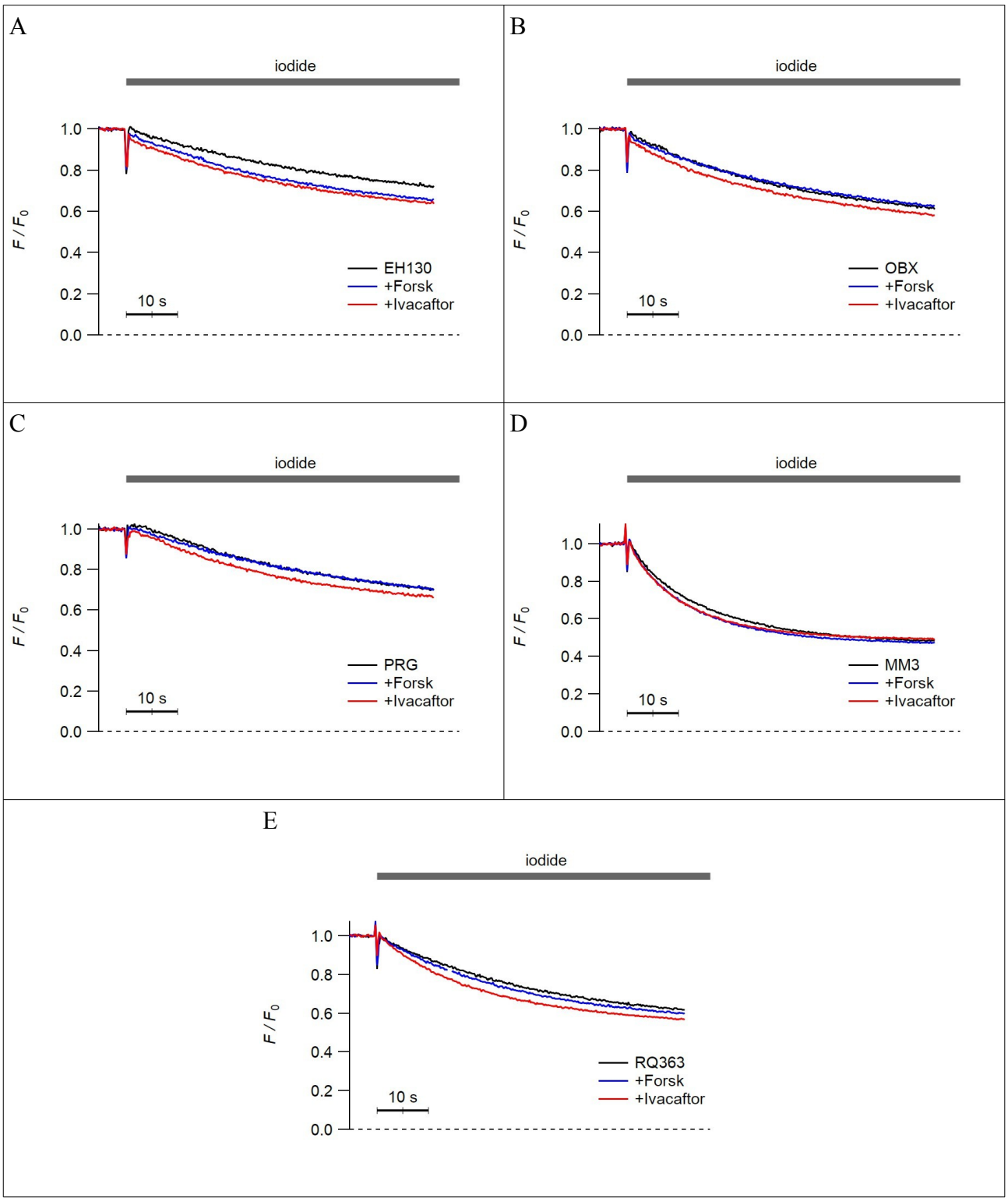

Figure S18. Anionophore-driven iodide transport in cells transfected with F508del CFTR. Figure indicate the time course of the fluorescence decay in mutant-CFTR transfected FRT cells incubated with 2 μM of anionophores. Iodide transport was measured after incubation with anionipore (black trace), anionophore plus forskolin that activates the mutant-CFTR (blue trace) and in cells pre-treated with the corrector lumacaftor for 24 hours, and incubated with anionophore and forskolin (red line).

REFERENCES

Altomare A, Burla MC, Camalli M, et al (1999) SIR97: a new tool for crystal structure determination and refinement. J Appl Crystallogr 32:115–119. doi: 10.1107/S0021889898007717

Farrugia LJ (1999) WinGX suite for small-molecule single-crystal crystallography. J Appl Crystallogr 32:837–838. doi: 10.1107/S0021889899006020

Hübschle CB, Sheldrick GM, Dittrich B (2011) ShelXle: a Qt graphical user interface for SHELXL. J Appl Crystallogr 44:1281–1284. doi: 10.1107/S0021889811043202

Kancharla P, Reynolds KA (2013) Synthesis of 2,2′-bipyrrole-5-carboxaldehydes and their application in the synthesis of B-ring functionalized prodiginines and tambjamines. Tetrahedron 69:8375–8385. doi: 10.1016/j.tet.2013.07.067